stichting
mathematisch
centrum

MC

AFDELING NUMERIEKE WISKUNDE NW 97/80 DECEMBER
(DEPARTMENT OF NUMERICAL MATHEMATICS)

M. BAKKER & D. HOONHOUT

NUMERICAL SOLUTION OF A DIFFUSION PROBLEM WITH SEGREGATION AT A MOVING INTERFACE

Preprint

kruislaan 413 1098 SJ amsterdam

Printed at the Mathematical Centre, 413 Kruislaan, Amsterdam.

The Mathematical Centre, founded the 11-th of February 1946, is a non-profit institution aiming at the promotion of pure mathematics and its applications. It is sponsored by the Netherlands Government through the Netherlands Organization for the Advancement of Pure Research (Z.W.O.).

1980 Mathematical subject classification: 65N30; CR5.17

Numerical solution of a diffusion problem with segregation at a moving interface [*)]

by

M. Bakker & D. Hoonhout [**)]

ABSTRACT

The transport of impurities implanted in silicon, which accompanies the annealing of implantation damage by means of pulsed-laser irradiation, is described by a one-dimensional diffusion equation whose solution is discontinuous at a moving interior point. This discontinuity is due to seggregation of mass at the liquid/solid interface during (re)solidification. This paper describes the pitfalls the numerical analyst will encounter and how he can cope with them.

KEY WORDS & PHRASES: *moving-boundary problem, diffusion problem, finite-difference methods, Runge-Kutta-Chebyshev methods, ordinary differential equation*

[*)] This report will be submitted for publication elsewhere.

[**)] FOM-Instituut voor Atoom- en Molecuulfysica

1. INTRODUCTION

The introduction of dopant atoms in silicon is normally accomplished via diffusion or via ion implantation. In the latter case, a monoenergetic beam of ionized dopant atoms, accelerated to an energy in the range 10-500 keV, is directed onto a monocrystalline silicon target. Thus the dopant atoms penetrate the silicon to depths in the order of 10-500 nm in a well controlled manner. However, ion implantation introduces a high degree of disorder in the surface layer of the silicon crystal. Therefore, an annealing procedure is needed to restore the crystallographic structure of the implanted layer and to make the implanted dopant atoms electrically active.

Traditionally, this is done by a prolonged thermal treatment at 700-1100°C. A new, promising approach to the annealing problem is the irradiation of the implanted silicon with a pulsed high-power laser, mostly a Q-switched ruby- or Nd:YAG-laser. It is found that after pulsed-laser annealing the crystallinity of the implanted layer is restored, but the depth distribution of the dopant has changed drastically [3,4]. One model to explain this is laser-induced melting of the implanted layer followed by rapid resolidification during cool-down. In this picture, the high diffusivity in liquid silicon, and the segregation of dopant atoms at the moving solidification front are held responsible for the changes in the dopant depth distribution.

This paper describes a numerical solution of a mathematical model for solute diffusion in the liquid and segregation at the phase boundary. A comparison between this model and experimental dopant profiles, measured after pulsed ruby-laser annealing has been published elsewhere [2,3].

In previous computer models, presented by Baeri et al. [1] and White et al. [7], segregation and diffusion in the liquid are represented as separate steps, although it is probably more realistic to have both effects interact continuously. It is not clear in these models which boundary conditions at the walls separating the liquid from the solid and from the vacuum are used to solve the diffusion equation. Furthermore, it is not clear how the width of the intervals, in which the depth scale is divided, affects the results. These questions are answered explicitly for our computer model.

As the material is implanted and laser-irradiated over an area of the order of a few cm^2, which is extremely large compared to the depth range of the implantation, we can describe the physical process as a one-dimensional problem. The mathematical model can be described as follows. Let $C(x,t)$ be the depth distribution of the dopant as function of the depth x and the time t. Prior to laser-annealing, $C(x,t)$ can be approximated by a Gaussian distribution with its peak at depth R_p and with standard deviation ΔR_p. Due to the laser-pulse, a melt front moves from the surface at $x = 0$ to a maximum molten depth a. Usually, $a >> R_p$. As it was seen that the rate of melting has very little influence, we will assume that the material melts down to $x = a$ instantaneously at time $t = 0$. During cool-down, the resolidification front moves back from $x = a$ to $x = 0$ at a velocity v which is assumed to be constant. Thus the position of the front is given by $g(t) = a - vt$. At the resolidification front, the dissolved dopant atoms segregate in such a way that the ratio of the concentration in liquid and solid in the immediate vicinity of the front is equal to k, the interfacial distribution coefficient. It is assumed that k is constant during the process while we will only consider cases for which $k < 1$. In the liquid phase, the dopant atoms diffuse according to a diffusion coefficient D. On the time-scale of pulsed-laser annealing, solute diffusion in the solid can be neglected.

Thus, the calculation of the dopant depth distribution $C(x,t)$ after completion of the process boils down to the solution of the one-dimensional diffusion equation

$$(1.1) \qquad \frac{\partial C}{\partial t} = D \frac{\partial^2 C}{\partial x^2} \; ; \qquad 0 < x < g(t),$$

with

$$(1.2) \qquad g(t) = a - vt.$$

The absence of diffusion in the solid phase implies

$$(1.3) \qquad \frac{\partial C}{\partial t} = 0; \; g(t) < x < a.$$

The boundary, initial and interface conditions are the following

a) for t = 0, the depth distribution for all x in the region $0 \leq x \leq a$ is a Gaussian function with its maximum at $x = R_p$ and a standard deviation ΔR_p. In formula

$$(1.4) \qquad C(x,0) = \exp(-(\frac{x-R_p}{\Delta R_p})^2/2);$$

b) no mass transport across the vacuum-liquid interface is allowed:

$$(1.5) \qquad \frac{\partial C}{\partial x} = 0; \; x = 0, \; t > 0;$$

c) the segregation taking place at the resolidification front at $x = g(t)$ is expressed as

$$(1.6) \qquad \lim_{x \downarrow g(t)} C(x,t) = k \lim_{x \uparrow g(t)} C(x,t), \qquad t > 0.$$

As a measure of segregation we compute the so-called surface fraction F(s) defined by

$$(1.7) \qquad F(s) = \frac{\int_0^s C(x,t)dx}{\int_0^a C(x,t)dx},$$

where we choose

$$(1.8) \qquad \begin{array}{l} s < < a; \\ t \geq \frac{a-s}{v}, \end{array}$$

i.e. we compute the amount of mass in the region [0,s] after resolidification. In this paper, we always chose the values

$$\begin{aligned} &s = 240\ \mathring{A}\ ; \\ (1.9)\qquad &a = 3000\ \mathring{A}; \\ &v = 4\text{m/s}; \end{aligned}$$

but the user is enabled to give other values on the input record.

ACKNOWLEDGEMENTS

The authors wish to thank Prof. Kistemaker of Stichting FOM and Prof. Baayen of Stichting Mathematisch Centrum for their assistance. This work was made possible by Stichting FOM, Stichting Mathematisch Centrum and Nederlandse Organisatie voor zuiver-wetenschappelijk onderzoek (ZWO).

2. NUMERICAL ANALYSIS OF THE PROBLEM

In this chapter we discuss the several difficulties and pitfalls predictable or not which are met during the process of numerically solving the problem. To that end, we first scale the problem by the introduction of the dimensionless variables

$$(2.1)\qquad \rho = \frac{x}{a}\ ;\ \alpha = \frac{D}{av}\ ; \qquad \tau = \frac{D}{a^2}\, t;\ \mu = \frac{R_p}{a}\ ;\ \sigma = \frac{\Delta R_p}{a}\ .$$

Scaling of (1.1-1.6) by (2.1) leads to the dimensionless problem (with $c(\rho,\tau) = C(\rho a, \alpha^2 \tau D^{-1})$)

$$(2.2a)\qquad \frac{\partial c}{\partial \tau} = \begin{cases} 0 & , 1 - \alpha\tau < \rho \le 1; \\ \dfrac{\partial^2 c}{\partial \rho^2} & , 0 \le \rho < 1 - \alpha\tau; \end{cases} \qquad 0 \le \tau \le \alpha^{-1};$$

with boundary conditions

(2.2b)
$$\frac{\partial c}{\partial \rho} = 0, \ \rho = 0;$$
$$\lim_{\rho \downarrow 1-\alpha\tau} c = k \lim_{\rho \uparrow 1-\alpha\tau} c, \qquad \tau > 0.$$

and initial conditions

(2.2c) $$c(\rho,\tau) = \exp(-\tfrac{1}{2}(\frac{\rho-\mu}{\sigma})^2)$$

2.1. Derivation of a mixed boundary condition at the interface

From a mathematical point of view, (2.2) is incomplete since the boundary and initial conditions (2.2b-2.2c) are insufficient. However, we can use the additional external condition

(2.3) $$\int_0^1 c(\rho,\tau)d\rho = \int_0^1 c(\rho,0)d\rho, \qquad \tau \geq 0,$$

which can physically be interpreted as the conservation of mass during the resolidification process. This means that

(2.4) $$\frac{d}{d\tau} \int_0^1 c(\rho,\tau)d\rho = 0, \qquad \tau \geq 0.$$

Further elaboration of (2.4) yields, if we substitute $g(\tau) = 1 - \alpha\tau$, and use (2.2a-2.2b)

$$\frac{d}{d\tau}\left[\int_0^{g(\tau)} c(\rho,\tau)d\rho + \int_{g(\tau)}^1 c(\rho,\tau)d\rho\right] =$$

(2.5)
$$= \frac{dg}{d\tau} \lim_{\rho \uparrow g(\tau)} c(\rho,\tau) + \int_0^{g(\tau)} \frac{\partial c}{\partial \tau}(\rho,\tau)d\rho$$
$$- \frac{dg}{d\tau} \lim_{\rho \downarrow g(\tau)} c(\rho,\tau) + \int_{g(\tau)}^1 \frac{\partial c}{\partial \tau}(\rho,\tau)d\rho =$$

$$= \frac{dg}{d\tau}(1-k) \lim_{\rho \uparrow g(\tau)} c + \int_0^{g(\tau)} \frac{\partial^2 c}{\partial \rho^2}(\rho,\tau)d\rho =$$

$$= \frac{dg}{d\tau}(1-k) \lim_{\rho \uparrow g(\tau)} c + \lim_{\rho \uparrow g(\tau)} \frac{\partial c}{\partial \rho} = 0.$$

Since $g(\tau) = 1 - \alpha\tau$, we have the mixed boundary condition

$$\text{(2.2d)} \qquad \lim_{\rho \uparrow 1-\alpha\tau} \frac{\partial c}{\partial \rho} = \alpha(1-k) \lim_{\rho \uparrow 1-\alpha\tau} c,$$

which makes the initial boundary problem complete.

2.2. Semi-discretization in the space variable

We divide the interval [0,1] in N segments of equal length (see Figure 1).

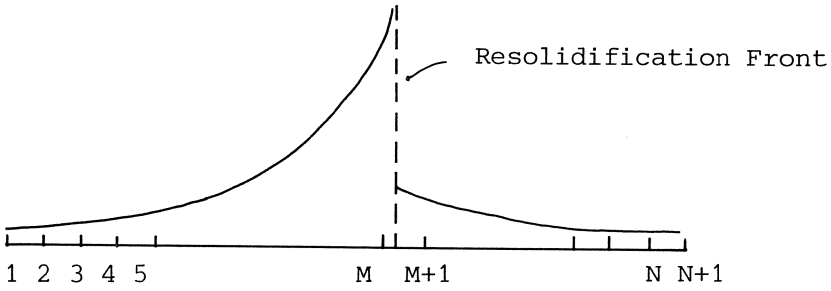

Figure 1; Graph of $c(\rho,\tau)$

At time τ, the interface is situated in the interval $[\rho_M,\rho_{M+1}]$ with

$$\text{(2.6)} \qquad \begin{aligned} \rho_i &= h(i-1),\ i = 1,\dots,N+1;\ h = 1/N \\ M &= [1+N(1-\alpha\tau)]. \end{aligned}$$

Let $c(\rho_i,\tau) \simeq c_i(\tau)$, $i = 1,\dots,N+1$.

For $i = 1,\dots,M-1$, we use the standard finite difference approximation [2] for (2.2a)

$$\frac{dc_i}{d\tau} = \frac{c_{i-1}-2c_i+c_{i+1}}{h^2}, \quad i = 2,\ldots,M-1;$$

(2.7a)

$$\frac{dc_1}{d\tau} = \frac{2}{h^2}(c_2-c_1).$$

For i > M, it is also simple:

$$\text{(2.7b)} \qquad \frac{dc_i}{d\tau} = 0, \quad i > M.$$

For i = M, approximation of $dc_M/d\tau$ is more problematic, since c is discontinuous on $[\rho_M,\rho_{M+1}]$.

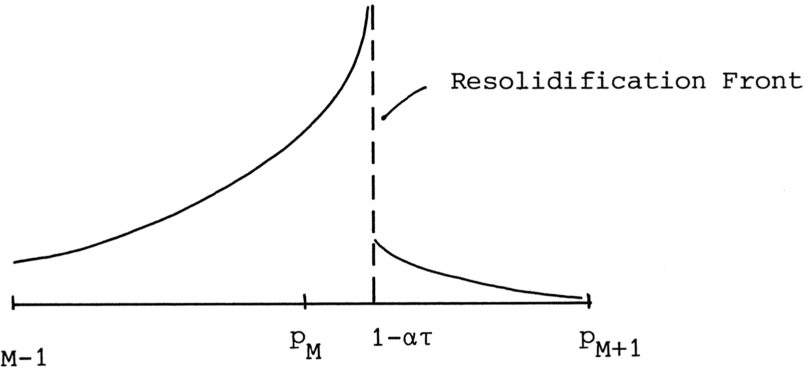

Figure 2.

In order to get a suitable approximation of $\frac{\partial^2 c}{\partial \rho^2}$ at $\rho = \rho_M$, we put

$$\delta = 1 - \alpha\tau - \rho_M;$$

(2.7c)

$$\frac{\partial^2 c}{\partial \rho^2}(\rho_M,\tau) \simeq \omega_1\, c(\rho_{M-1},\tau) + \omega_2\, c(\rho_M,\tau) + \omega_3\, c(\rho_M+\delta,\tau)$$

where ω_1,ω_2 and ω_3 are chosen in such a way that (2.7c) has maximum accuracy, hence we find

$$\omega_1 = \frac{2}{h(h+\delta)}\ ;\ \omega_3 = \frac{2}{\delta(h+\delta)}$$

(2.8)

$$\omega_2 = -\ \omega_1 - \omega_3,\quad 0 < \delta < h.$$

The crucial question is: how to compute $c(\rho_M+\delta,\tau)$?
We do this by extrapolation. Let c_{int} be the (unknown) approximation of $c(\rho_M+\delta,\tau)$. On the interval $[\rho_{M-1},\rho_M+\delta]$ we define a parabola which interpolates $c(\rho,\tau)$ at the points ρ_{M-1},ρ_M and $\rho_M+\delta$, and which satisfies (2.2d). In formula

(2.9)

$$\begin{aligned} c(\rho,\tau) \simeq \hat{c}(\rho,\tau) &= \frac{(\rho-\rho_M)(\rho-\rho_M-\delta)}{h(h+\delta} c(\rho_{M-1},\tau) + \\ &+ \frac{(\rho-\rho_{M-1})(\rho_M+\delta-\rho)}{h\delta} c(\rho_M,\tau) + \\ &+ \frac{(\rho-\rho_M)(\rho-\rho_{M-1})}{\delta(h+\delta)} c_{int};\ \rho \in [\rho_{M-1},\rho_M+\delta]; \\ \frac{\partial\hat{c}}{\partial\rho} &= \alpha(1-k)c_{int},\ \rho = \rho_M + \delta. \end{aligned}$$

Elaboration of (2.9) yields

$$c_{int} \simeq \frac{c(\rho_M,\tau) - \beta^2 c(\rho_{M-1},\tau)}{1-\beta^2-\alpha(1-k)3h}\ ,\quad \beta = \frac{\delta}{h+\delta}\ . \tag{2.10}$$

At the other hand, if $\delta \to h$, it is better to approximate c_{int} by linear extrapolation of $c(\rho_{M+1},\tau)$ and $c(\rho_{M+2},\tau)$ provided, of course, that $M \leq N-1$. This means that

$$c_{int} \simeq \frac{(2-\delta/h)c(\rho_{M+1},\tau)-(1-\delta/h)c(\rho_{M+2},\tau)}{k}\ . \tag{2.11}$$

Numerical experiments have shown that (2.10) should be applied if $\beta < 4/9$ and (2.11) otherwise.

Summarizing, we found for $dc_M/d\tau$ the formula

$$
(2.7d) \qquad \frac{dc_M}{d\tau} = \begin{cases} \dfrac{2}{h+\delta}\left[\dfrac{c_{M-1}-c_M}{h} + \dfrac{c_{int}-c_M}{\delta}\right], & \delta > 0; \\[2ex] \dfrac{2}{h}\left[\dfrac{c_{M-1}-c_M}{h} + \alpha(1-k)c_M\right], & \delta = 0, \end{cases}
$$

where c_{int} is defined by (2.10) or (2.11).

REMARK. In earlier versions of this program, c_{int} was approximated by linear interpolation between c_M and c_{M+1}/k. This approach was rather unsatisfactory, since the behaviour of $c(\rho,\tau)$ sometimes differs left and right of the interface (monotonicly increasing to the left and monotonicly decreasing to the right, see fig. 2) which resulted in a systematical underestimation of c_{int}. Because of this underestimation, relation (2.3) refused to remain valid; especially as α was large and k was small, the mass increased by about 15%, and much more if N was small.

2.3. Boundary layers; choice of N

It turns out that $c(\rho,\tau)$ has a boundary layer left of $1 - \alpha\tau$, if α is large and k small. Physically, this can be interpreted as a high concentration of mass near the resolidification front due to slow mass transport and strong segregation. One is forced to choose N large in this case. From (2.10) we can derive a minimum value of N in order to keep the denominator of (2.10) positive, i.e.

$$
(2.12) \qquad N > \frac{\alpha(1-k)\beta}{1-\beta^2}, \quad 0 \le \beta \le \tfrac{1}{2}.
$$

This is the minimum value of N. In practice N should be much larger, certainly if k is small and α large; a safe choice would be

$$
(2.13) \qquad N \sim \frac{\alpha}{5k}.
$$

2.4. Integration of semi-discretized problem

In this section, we discuss the organizatory problems which are encountered if we want to solve (2.7) by an ODE integrator.

As we saw in §2.2, we can consider (2.7) as a system of ODE's with dimension decreasing in time

$$\text{(2.14)} \qquad M(\tau) = \text{entier}((1-\alpha\tau)*N)+1, \quad 0 \le \tau < \alpha^{-1}.$$

If we treat (2.7) as a system of fixed length by putting $dc_i/d\tau = 0$, $i > M$ and let a common ODE integrator loose on it, we run into trouble and the output results are rubbish.

The explanation is simple. Let $\{\tau_i\}_{i=1}^{N}$ be a set of time-points defined by

$$\tau_i = \frac{i-1}{\alpha N} = \Delta\tau(i-1), \quad i = 1,\ldots,N.$$

If $\tau_i \le \tau < \tau_{i+1}$, the de facto dimension of (2.7) is N+1-i. If τ passes τ_{i+1}, the dimension of (2.7) is diminished by one, c_{N+1-i} is multiplied by k and kept constant forever etc. An ODE integrator may choose step-sizes of the time-step which exceed $\Delta\tau$ by an order of magnitude. By this choice several points τ_i are passed in one integration step. This is an invitation to disaster, which duly materializes. Hence we impose

<u>CONDITION 1</u>. The ODE integrator should hop from one time-point τ_i to the next, after which c_{N+1-i} is multiplied by k and kept constant.

The above precaution alone is insufficient because many ODE integrators do not really hit the end-point of the integration interval but go on until it is passed and then interpolate between the last and previous time-points. This also leads to disaster so we impose

<u>CONDITION 2</u>. The ODE integrator should hit the end-point exactly. In formula, at time τ, $\tau_i \le \tau < \tau_{i+1}$

$$\text{STEPSIZE} = \min(\Delta^*\tau \ , \ \tau_{i+1}-\tau)$$

where $\Delta^*\tau$ is a stepsize computed on the basis of accuracy, stability and possibly other motives as well.

Because most ODE integrators do not satisfy condition 2, we took a house ODE integrator which uses explicit one-step multi-point Runge-Kutta-Chebyshev methods of second order consistency and applies automatic step-size control based upon accuracy and stability [5]. With a slight alteration condition 2 could be implemented in the package RKC. This delivered very satisfactory results.

REMARK. In an earlier stage, we worked with the forward Euler method [6,p.316] with constant time-step $\Delta\tau = (m\alpha N)^{-1}$, where $m = 1+2N/\alpha$; in formula

$$(2.15) \qquad c_j(\rho,\tau+\Delta\tau) = c_j(\rho,\tau) + \Delta\tau \frac{d}{d\tau} c_j(\rho,\tau)$$

This simple algorithm satisfied the two above conditions. It was, however, too inaccurate, which was proved when the quotient

$$(2.16) \qquad Q(\tau) = \frac{\int_0^1 c(\rho,\tau)d\rho}{\int_0^1 c(\rho,0)d\rho}$$

was computed. According to (2.3) Q should be 1, but as $\tau \to \alpha^{-1}$, Q took unacceptable values, especially if α was large and k small. So we had to use a more sophisticated integrator. Experiments with RKC showed that the deviation of Q from unity was of the same order or magnitude as the relative tolerance for the time-integration.

3. DESCRIPTION OF THE PROGRAM

In this §, we give a brief description of the subroutine DRIVE and other subprograms (see Fig.3). For a more detailed description, we refer to the comment lines in the softward package.

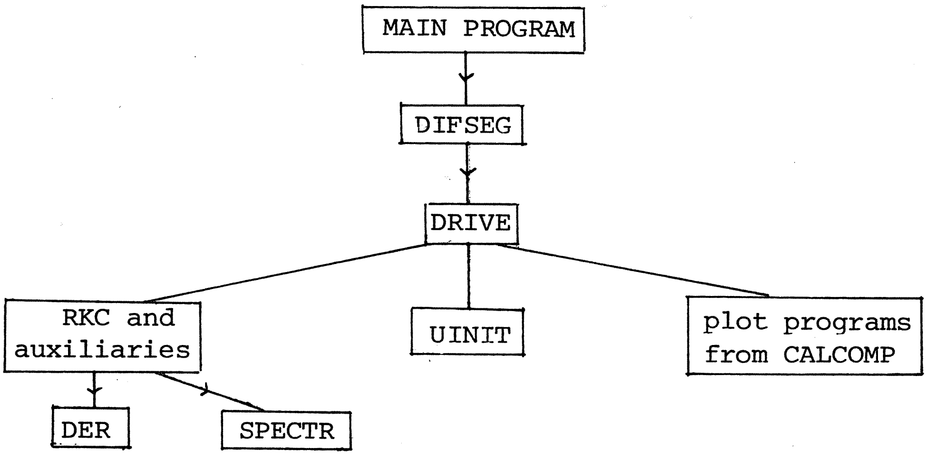

Figure 3; organization scheme of program

MCFOM - This is the main program to be written by the user; it should contain a blank common block of at least 7N + 13 words, where N is the number of segments; see §2; its only statement is a call of DIFSEG with the dimension of the blank common block as actual parameter;

DIFSEG - This subroutine reads and prints the input record and calls DRIVE if the work-space is large enough; otherwise it terminates the program printing a message of the reason;

DRIVE - This is the managing subroutine; it initializes $c(\rho,0)$ at the mesh-points, integrates (2.7) until the interface has passed 240 Å; after the integration, it computes the surface fraction and $Q(\tau)$; if desired, it plots $C(x,t)$ a couple of times together with a graph of the solid state;

RKC - This routine and its auxiliary routines perform the time-integration;

DER - This routine evaluates the vector $d\vec{c}/d\tau$, given an input vector $\vec{c}$ at time τ according to (2.7). It is called by RKC and its auxiliary routines;

SPECTR - This function is assigned the value of the spectral radius of the Jacobian matrix $(\partial \dot{c}_i/\partial c_j)$. Knowledge of this value is essential to numerically stable time-integration (see [5]);

UINIT - A function subprogram to be implemented by the user, which gives C(x,0) its value for given x.

4. THE INPUT RECORD

See the comment lines in subroutine DIFSEG.

5. WORKSPACE

In the main program a blank common block of length at least 7N+13 should be declared. This length should also be the actual parameter of DIFSEG.

6. COMMON BLOCKS

See the comment lines in subroutine DIFSEG.

7. TEST-EXAMPLES

The program was run for two sets of input values (see Table I) and a plot was drawn (see figs. 4-7). We see the curves become steeper and steeper as the resolidification front moves to the left.

s	240 Å	
D	1.e-4cm^2/s	5.e-4cm^2/s
a	3000 Å	
v	4 m/s	
N	500	
PLOT?	yes	
k	0.05	0.1
R_p	1100 Å	
ΔR_p	500 Å	

TABLE I; input records for test examples

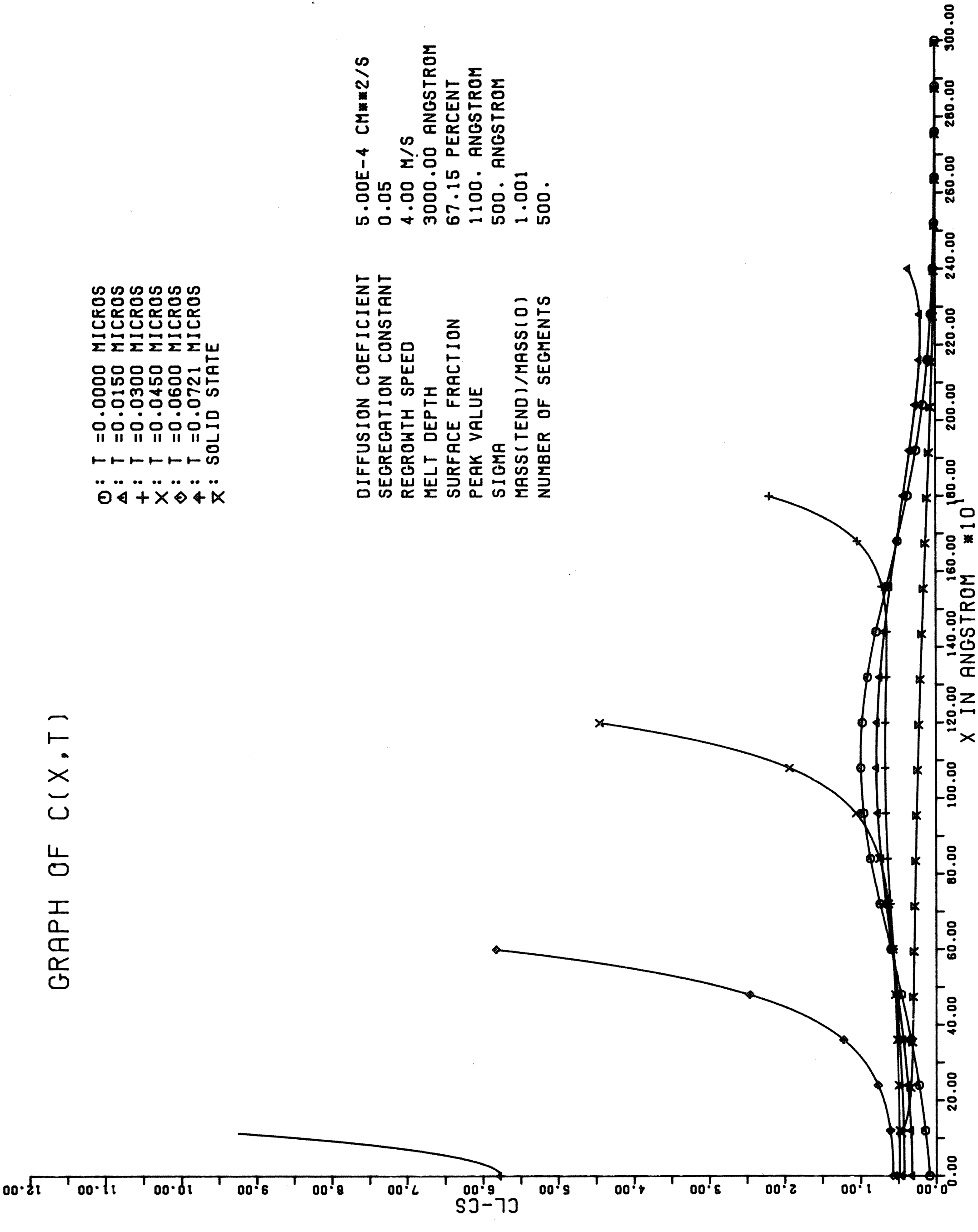
GRAPH OF C(X,T)
Θ: T =0.0000 MICROS
△: T =0.0150 MICROS
+: T =0.0300 MICROS
X: T =0.0450 MICROS
◇: T =0.0600 MICROS
✦: T =0.0721 MICROS
⋊: SOLID STATE
DIFFUSION COEFICIENT 5.00E-4 CM**2/S
SEGREGATION CONSTANT 0.05
REGROWTH SPEED 4.00 M/S
MELT DEPTH 3000.00 ANGSTROM
SURFACE FRACTION 67.15 PERCENT
PEAK VALUE 1100. ANGSTROM
SIGMA 500. ANGSTROM
MASS(TEND)/MASS(0) 1.001
NUMBER OF SEGMENTS 500.
CL-CS
0.00
1.00
2.00
3.00
4.00
5.00
6.00
7.00
8.00
9.00
10.00
11.00
12.00
X IN ANGSTROM *10¹
0.00
20.00
40.00
60.00
80.00
100.00
120.00
140.00
160.00
180.00
200.00
220.00
240.00
260.00
280.00
300.00

figure 4

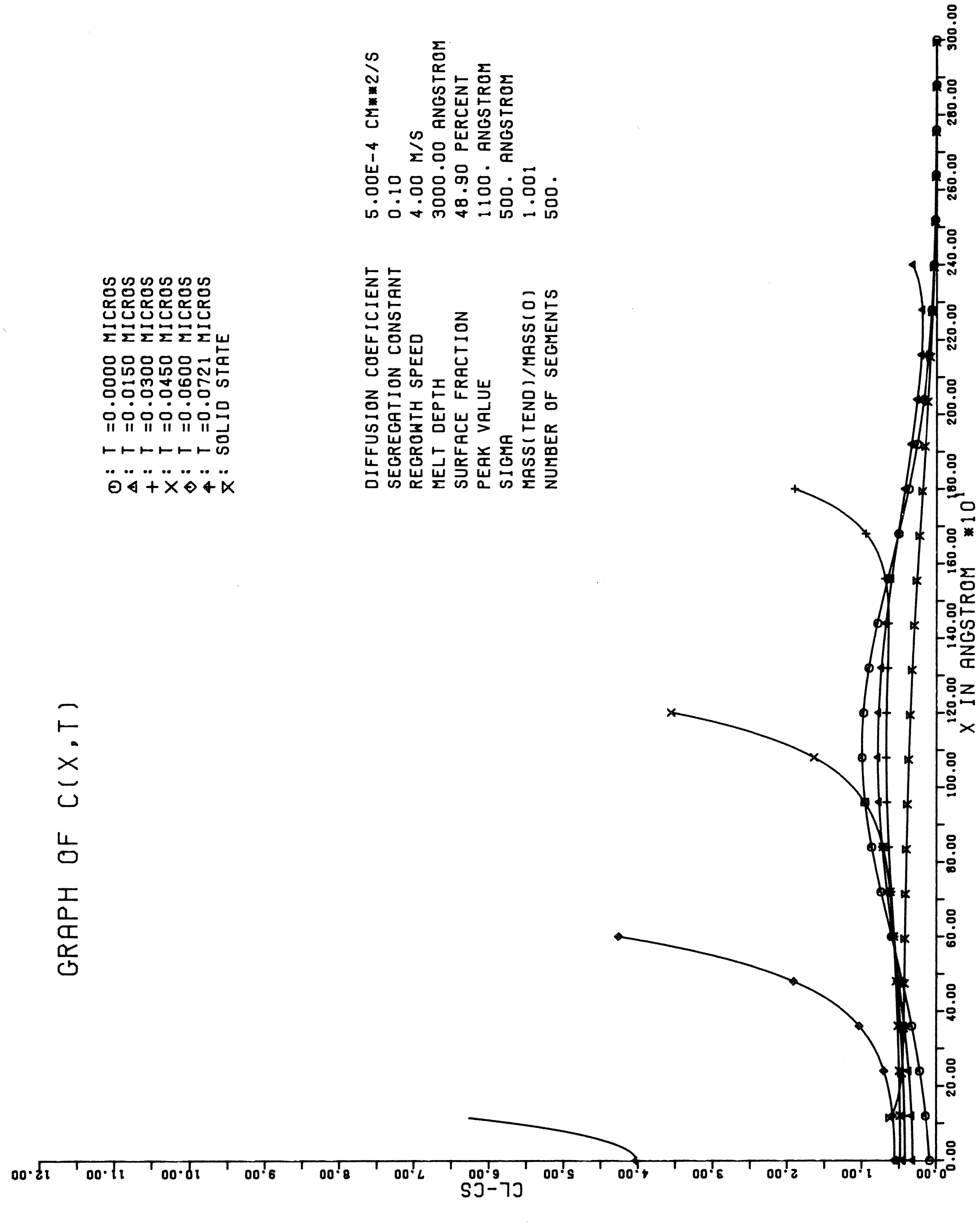
GRAPH OF C(X,T)
Θ : T =0.0000 MICROS
△ : T =0.0150 MICROS
+ : T =0.0300 MICROS
X : T =0.0450 MICROS
◇ : T =0.0600 MICROS
✦ : T =0.0721 MICROS
✗ : SOLID STATE
DIFFUSION COEFICIENT 5.00E-4 CM**2/S
SEGREGATION CONSTANT 0.10
REGROWTH SPEED 4.00 M/S
MELT DEPTH 3000.00 ANGSTROM
SURFACE FRACTION 48.90 PERCENT
PEAK VALUE 1100. ANGSTROM
SIGMA 500. ANGSTROM
MASS(TEND)/MASS(0) 1.001
NUMBER OF SEGMENTS 500.
CL-CS
0.00
1.00
2.00
3.00
4.00
5.00
6.00
7.00
8.00
9.00
10.00
11.00
12.00
X IN ANGSTROM *10¹
0.00
20.00
40.00
60.00
80.00
100.00
120.00
140.00
160.00
180.00
200.00
220.00
240.00
260.00
280.00
300.00

figure 5

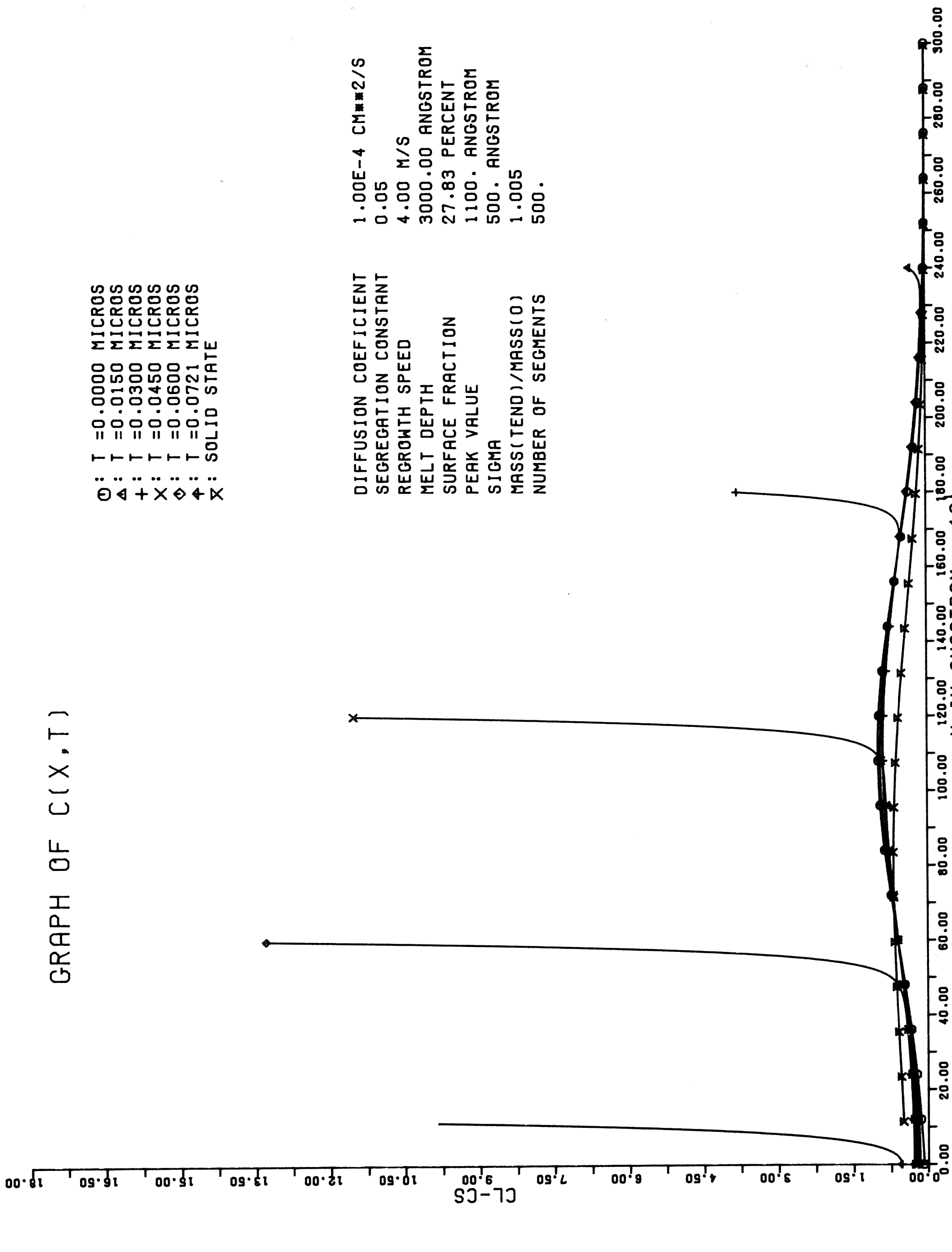
GRAPH OF C(X,T)
⊖: T =0.0000 MICROS
△: T =0.0150 MICROS
+: T =0.0300 MICROS
X: T =0.0450 MICROS
◇: T =0.0600 MICROS
✦: T =0.0721 MICROS
X: SOLID STATE
DIFFUSION COEFICIENT 1.00E-4 CM**2/S
SEGREGATION CONSTANT 0.05
REGROWTH SPEED 4.00 M/S
MELT DEPTH 3000.00 ANGSTROM
SURFACE FRACTION 27.83 PERCENT
PEAK VALUE 1100. ANGSTROM
SIGMA 500. ANGSTROM
MASS(TEND)/MASS(0) 1.005
NUMBER OF SEGMENTS 500.
CL-CS
0.00
1.50
3.00
4.50
6.00
7.50
9.00
10.50
12.00
13.50
15.00
16.50
18.00
X IN ANGSTROM *10¹
0.00
20.00
40.00
60.00
80.00
100.00
120.00
140.00
160.00
180.00
200.00
220.00
240.00
260.00
280.00
300.00

figure 6

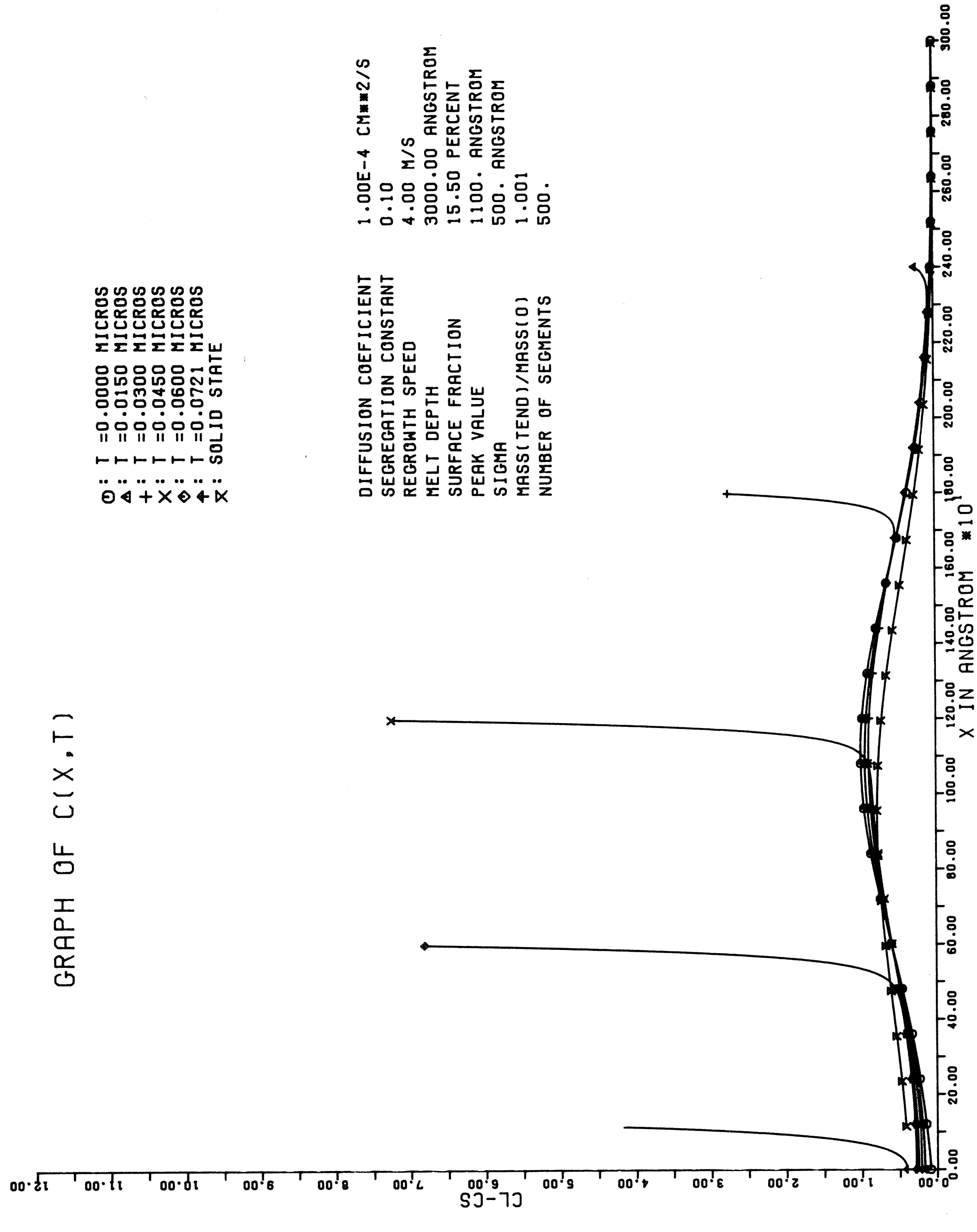
GRAPH OF C(X,T)
⊖ : T =0.0000 MICROS
△ : T =0.0150 MICROS
+ : T =0.0300 MICROS
X : T =0.0450 MICROS
◇ : T =0.0600 MICROS
✦ : T =0.0721 MICROS
⧖ : SOLID STATE
DIFFUSION COEFICIENT 1.00E-4 CM**2/S
SEGREGATION CONSTANT 0.10
REGROWTH SPEED 4.00 M/S
MELT DEPTH 3000.00 ANGSTROM
SURFACE FRACTION 15.50 PERCENT
PEAK VALUE 1100. ANGSTROM
SIGMA 500. ANGSTROM
MASS(TEND)/MASS(O) 1.001
NUMBER OF SEGMENTS 500.
CL-CS
0.00
1.00
2.00
3.00
4.00
5.00
6.00
7.00
8.00
9.00
10.00
11.00
12.00
X IN ANGSTROM *10¹
0.00
20.00
40.00
60.00
80.00
100.00
120.00
140.00
160.00
180.00
200.00
220.00
240.00
260.00
280.00
300.00

figure 7

LITERATURE

[1] P. BAERI, S.U. CAMPISANO, G. FOTI, E. RIMINI, Physical review letters 41 (1978), p.2346 ff.

[2] G.E. FORSUTHE and W.R. WASOW, *Finite difference methods for partial differential equations,* Wiley and Sons, Inc., New York, 1960.

[3] D. HOONHOUT, Y. TAMMINGA, R. GARRETT, F.W. SARIS, From the proceedings of the conference on *Laser effects in ion-implanted semiconductors,* University of Catania (Italy), 1978.

[4] D. HOONHOUT, F.W. SARIS, submitted to J. Appl. Phys.

[5] B.P. SOMMEIJER & P.J. VAN DER HOUWEN, *On the economization of stabilized Runge-Kutta methods with applications to parabolic initial value problems,* to appear in Zeitschrift für angewandte Mathematik und Mechanik.

[6] J. TODD, editor, *A survey of numerical analysis,* McGraw-Hill, Inc., New York, 1962.

[7] C.W. WHITE, S.R. WILSON & B.R. APPLETON, F.W. YOUND, *Supersaturated substitutional alloys formed by ion implantation and pulsed laser annealing of group III and group V dopants in silicon,* J. Appl. Phys. 51 (1980), p.738 ff.